Research article

An approach to modelling and simulation of single-walled carbon nanocones for sensing applications

Bhavik Ardeshana *, Umang Jani, Ajay Patel, and Anand Joshi

Mechatronics Department, G.H. Patel College of Engineering and Technology, Vallabh-Vidyanagar, Gujarat-388120, India

* Correspondence: Email: ardeshanabhavik@gmail.com.

Abstract: In the present manuscript an approach to modelling and simulation of nanocones has been suggested for their use as sensing mediums. The vibrational behaviours of bridged and cantilever Single-Walled Carbon nanocones are modelled using three-dimensional elastic beams of carbon-carbon bonds and atomic masses. Also, the dynamic analysis of bridged and cantilever configurations of these nanocones with different disclination angles of $60°$, $120°$, $180°$, and $240°$ is performed to evaluate the variation in stiffness with different configurations. The analysis also exhibits the effect of change in the length of nanocones on the vibrational frequencies. For the said purpose a mass equivalent to a carbon atom has been added at the nodes. It is observed that increasing side length of a Single-Walled Carbon nanocones with a constant apex angle results in a reduction in the fundamental frequency. It is also clear from the results that Single-Walled Carbon nanocones with larger apex angles exhibit smaller values of fundamental frequencies. The results suggest that smaller lengths of nanocones are better candidates for sensing applications as they exhibit substantial change in the fundamental frequencies. It can be stated that with higher number of bonds and atoms Single-Walled Carbon nanocones undergoes substantial bending with large declination angle which can be considered as an important finding.

Keywords: SWCNC; finite element method; sensing; vibration analysis

1. Introduction

In recent times, dissimilar nanostructures such as carbon nanotubes (CNTs) [1], fullerenes [2], carbon nanorings [3], and carbon nanocones (CNCs) [4,5] have involved a great deal of interest for

evaluating the properties. Due to varied potential applications of single walled carbon nanocones (SWCNCs) in altered areas such as cold electron and field emitter [6], adsorbent [7], and mechanical sensors [8,9], a complete understanding of their mechanical, physical, and electronic properties is needed. The ultra-sensitivity of mass detectors was first investigated by using individual cantilevered single-walled carbon nanocone (SWCNC) resonators [9].

Krishnan et al. [10] investigated nanocones with different apex angles of 19.2 °, 38.9 °, 60 °, 84.6 °, and 112.9 ° using experiments. Consequently, Naess et al. [11] studied the morphologies of the CNCs with dissimilar apex angles by using transmission electron microscopy (TEM), synchrotron X-ray and electron diffraction.

Molecular dynamics (MD), virtual analysis [12,13] and density functional theory (DFT) [14] are the utmost important approaches, while the other approaches can be subdivided to Bernoulli-Euler/Timoshenko beam models [15,16,17], the shell models [18,19,20], the molecular structural models [21–24], and meshless approaches [25,26].

Yan et al. [27] studied the physical factors and flexible properties of SWCNCs by using the higher order continuum principle. They employed all five types of CNCs to test the influence of the conical angle on the mechanical properties. The model analysis performed SWCNTs and SWCNCs [28] using finite element method (FEM). In their work, natural frequencies and corresponding mode shapes of these nano structures were evaluated. Fakhrabadi et al. forecasted the elastic and buckling performance of CNCs with dissimilar sizes and vibrational properties [29,30]. Using the different sizes and boundary conditions, the elastic modulus and compressive forces of the axial buckling for CNCs were evaluated.

The three-dimensional vibrational mode shapes are excavated using the time histories of the three coordinates of each atom acquired from conducting one molecular dynamics simulation [31]. Huang et al. [32] evaluated CNCs which was used as a kind of novel and stable atomic force microscopy (AFM) tips because of their unique conical shape and high stability.

It has been observed in a number of manuscripts that understanding the vibration behaviours and dynamics at a nano level plays a very important role when these nanostructures are used as various sensors. Also based on the literature presented it is quite obvious that the work done in the proposed field of SWCNC is not substantial. Hence, in this manuscript, the authors have tried to propose a methodology for understating the structure and vibrational properties of nanocones by using an atomic scale finite element model based on molecular structural mechanics approach. The parameters evaluated for a nanocone include the boundary condition, apex angle and variation of lengths of SWCNCs. Simultaneously this study encompasses the effect of the stated parameters on the mode shapes and natural frequencies of single walled carbon nanocones. The SWCNCs with disclination angles of 60 °, 120 °, 180 °, and 240 ° with a cone height of 10 Å, 15 Å, and 20 Å each are considered.

In earlier studies, CNTs have been used for sensing applications. CNCs were made from the graphene sheet same as CNTs. CNC have different conical structure and vibrational properties, than CNTs. Therefore it is possible to use the CNC for different sensing applications. Patel et al. studied the vibrational characteristics of double walled carbon Nanotube (DWCNT), modelled using spring elements and lumped masses [33,34]. Simulations have been carried out to visualize the behaviour of DWCNTs subjected to different boundary conditions and when used as mass sensing devices.

2. Geometries Construction of SWCNCs

Natural cones have wide range of distribution of apex angle as reported [35], which can be used to explain a disclination model for cone-helix structures. The cone-helix model is effective in forecasting the anticipated apex angles of graphite cones produced under several laboratory settings and made naturally from fluids during metamorphism shape. There are five possible apex angles that are geometrically acceptable in relation to the condition of the Euler's theorem and the constriction of graphene as reported [36].

Nanocones have a sharp tip which can be used to determining the specific mechanical properties and because of that nanocones are very exciting materials for different types of application like technological. The angle of the sector removed from a flat graphene sheet to form a cone is known as disclination angle. Nanocones are classified according to their disclination angle. Authors have analysed carbon nanocone which have three different disclination angle $d_\theta = 60°$, $120°$, $180°$ and $240°$ with three different length of cone are 10 Å, 15 Å and 20 Å. These configurations further enhance the continuousness at the juncture of a graphene sheet. The studied nanocones with disclination angles of $60°$, $120°$, $180°$, and $240°$ are shown in Figure 1.
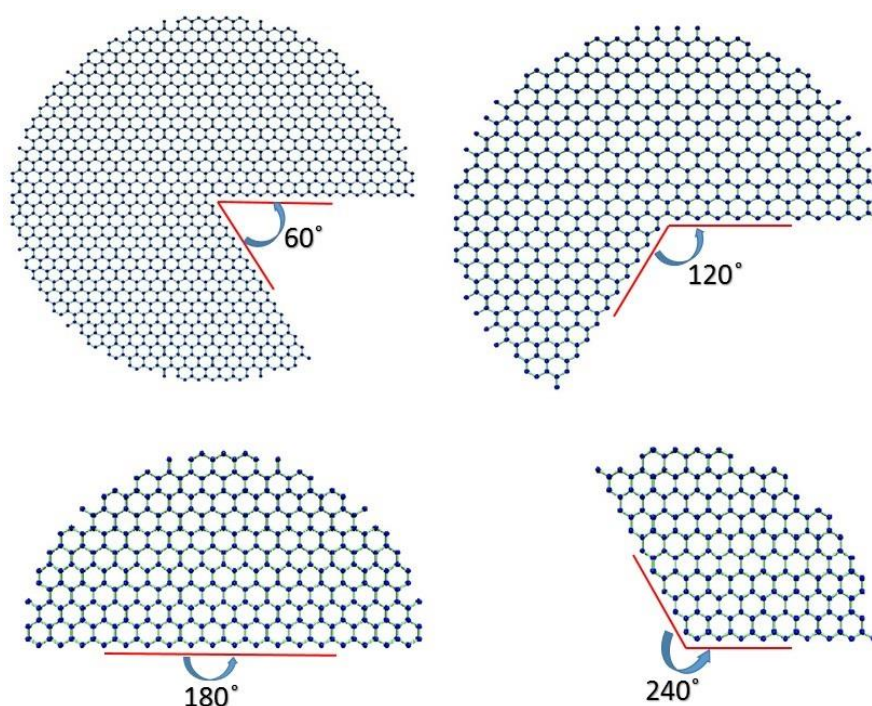
Figure 1. Cone sheets with disclination angles of $60°$, $120°$, $160°$, and $240°$.

The sliced graphene layer was created by removing the sector of the circular graphene sheet. Than the sliced layer was revolved by closing the angular gap so the nanocone is shaped. In a similar manner other graphene sheets were rotated over different constant angle so that new nanocones with different disclination angles are occurs.

Figure 2 shows formation of SWCNC from graphene sheet. The apex angles of cones are $112.9°$, $83.6°$, $60°$ and $38.9°$ respectively for the disclination angle $60°$, $120°$, $180°$ and $240°$. The apex angle of cones is obtained as $2\sin^{-1}(1-d_\theta/360)$.
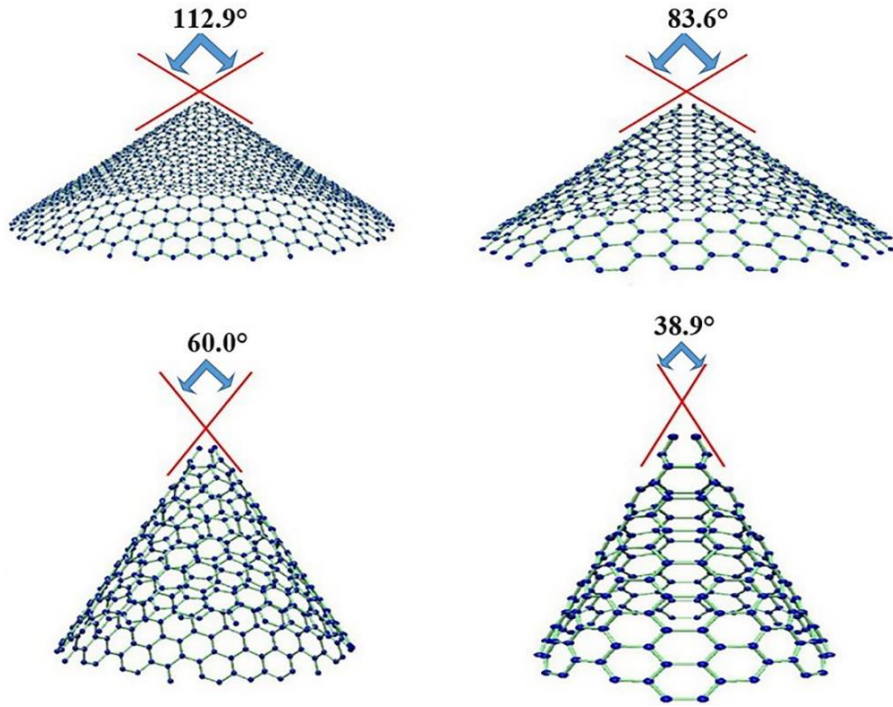
Figure 2. Cones with apex angles of 112.9 °, 83.6 °, 60 ° and 38.9 ° with cone heights of 20 Å.

The polar coordinate system convert into a three dimensional cone in Cartesian coordinate system shown in Figure 3 which transformation from graphene into a cone with disclination angle 240 °. The polar coordinates of point P, indicated in graphene division as (l, α), the parameters of graphene sector are L and φ. Sector OAB is bent at apex O where $\overline{OA}$ and $\overline{OB}$ lengths are same so, A point of $\overline{OA}$ length is touch to point B of $\overline{OB}$ length [19].
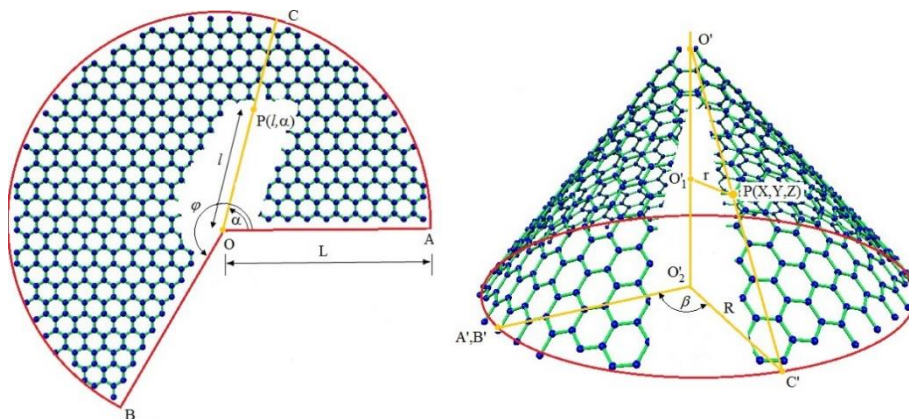
Figure 3. Symbols and variables used in the transformation from a graphene sheet for a cone 240 °.

Considering the point P(X,Y,Z), the following equations are obtained [27]:

$$X = r\cos\beta, \qquad Y = r\sin\beta, \qquad Z = -\sqrt{l^2 - r^2}, \tag{1}$$

where β and r are the unknown parameters. The graphene sheet transform from the three-dimensional cone and for that the relation between the corresponding angles as below:

$$\frac{\beta}{2\pi} = \frac{\alpha}{\phi} \tag{2}$$

From the Figure 3, the angle between $O'^2 O' C'$ and $O'^2 O' A'$ is the dihedral angle β, which can be found by rearranging the above Eq. (2) as below:

$$\beta = \alpha\left(\frac{2\pi}{\varphi}\right) \tag{3}$$

The relation between radiuses r and R with lengths l and L are as follow:

$$\frac{r}{R} = \frac{l}{L} \tag{4}$$

For obtaining the base radius R of cone by below Eq. (5)

$$R = \frac{L\varphi}{2\pi} \tag{5}$$

For finding the radius r, substitute the value of R from Eq. (5) to Eq. (4)

$$r = \frac{l}{2\pi} \tag{6}$$

For determining the point P in the three-dimensional cone just by substitute the value r and β from Eq. (6) and Eq. (3) respectively in Eq. (1) as follow:

$$X = \left(\frac{l\varphi}{2\pi}\right)\cos\left[\alpha\left(\frac{2\pi}{\varphi}\right)\right], \quad Y = \left(\frac{l\varphi}{2\pi}\right)\sin\left[\alpha\left(\frac{2\pi}{\varphi}\right)\right], \quad Z = -l\sqrt{1 - \left(\frac{\varphi}{2\pi}\right)} \tag{7}$$

Here, *X*, *Y* and *Z* indicate the atom coordinate of nanocone and angle are in radians.

3. Molecular Structural Mechanics Based Modelling of SWCNC

As per the MSM approach covalent bonds have been substituted as beam elements and the stiffness of the elements have been calculated by utilizing the process potential energy. The total force on individually atomic nuclei is the sum of the force produced by the electrons and

electrostatics force between the absolutely charged nuclei themselves. The overall formulation for the potential energy is

$$\Pi = \sum U_r + \sum U_\theta + \sum U_\phi + \sum U_\omega + \sum U_{vdw} \tag{8}$$

where U_r is the energy because of bond stretch interaction, U_θ is the energy because of bending (bond angle variation), U_ϕ is the energy because of dihedral angle torsion, U_ω is the energy because of out-of-plane torsion and U_{vdw} is the energy because of non-bonded van der Waals interaction.

$$U_r = \frac{1}{2} K_r (r - r_0)^2 = \frac{1}{2} K_r (\Delta r)^2 \tag{9}$$

$$U_\theta = \frac{1}{2} K_\theta (\theta - \theta_0)^2 = \frac{1}{2} K_\theta (\Delta \theta)^2 \tag{10}$$

$$U_\tau = U_\phi + U_\omega = \frac{1}{2} K_\tau (\Delta \phi)^2 \tag{11}$$

where K_r, K_θ and K_τ represent the bond stretching, bond bending and torsional resistance force constants, correspondingly, while $\Delta r, \Delta \theta$ and $\Delta \phi$ represent bond stretching increment, bond angle variation and angle variation of bond twisting, respectively.

As the potential energy in the two approaches is independent, energy equivalence of the stored energy of the two approaches, i.e., molecular mechanics and structural mechanics [24]

$$\frac{EA}{L} = K_r, \qquad \frac{EI}{L} = K_\theta, \qquad \frac{GJ}{L} = K_\tau \tag{12}$$

The elastic properties of the beam element are given as [24]

$$D = 4\sqrt{\frac{k_\theta}{k_r}}, \qquad E = \frac{k_r^2 L}{4\pi k_\theta}, \qquad G = \frac{k_r^2 k_\phi L}{8\pi k_\theta^2} \tag{13}$$

where D, L, E, I and G represent the diameter, length of cone, Young's modulus, moment of inertia and shear modulus of the beam element.

4. Modal Analysis of SWCNC

Here, the matrix equations are considered as the dynamic three-dimensional lumped model system. The equation of motion in a generalized form can be written as:

$$[M]\{\ddot{v}\} + [B]\{\dot{v}\} + [K]\{v\} = [F] \tag{14}$$

where $[M]$, $\{\ddot{v}\}$, $\{\dot{v}\}$, $[B]$, $[K]$ and $[F]$ indicate the global mass matrix, the second time derivative of the displacement vector $\{v\}$ (i.e., the acceleration), the velocity vector, global damping matrix, global stiffness matrix, and force vector respectively.

Utilizing the modal analysis the mode shape and natural frequency can be determined. In this study damping is overlooked. Hence, the new equation of motion without damping can be expressed in matrix notation for an undamped system is as follow:

$$[M]\{\ddot{v}\}+[K]\{v\}=\{0\} \tag{15}$$

Here the structural stiffness matrix $[K]$ does not include any pre-stress. Free vibration is harmonic for the linear system which can be considered in the following form:

$$\{v\}=\{\phi\}_i \cos \omega_i t \tag{16}$$

where the mode shape of ith natural frequency representing by vector $\{\phi\}_i$, the ith natural circular frequency is representing by the vector ω_i in radians per unit time, and t representing the time. Rewriting Equation (15) we get:

$$\left\{-\omega_i^2 [M]+[K]\right\}\{\phi\}_i=\{0\} \tag{17}$$

The equality of above equation (17) is satisfied by these two option, one option is $\{\phi\}_i=\{0\}$ and second option is $\left([K]-\omega^2 [M]\right)=0$. The first option is unimportant and therefore our interest is not in it. The second option gives the following answer

$$\left\|[K]-\omega^2 [M]\right\|=0 \tag{18}$$

This is an eigenvalue problem which may be solved for up to n values of ω^2 and n eigenvectors $\{\phi\}_i$ which satisfy Eq. (16), where n is the number of DOFs. The eigenvalue and eigenvector extraction techniques are used in the Block Lanczos method. Rather than outputting the natural circular frequencies $\{\omega\}$, the natural frequencies $\{f\}$ are output as

$$f_i=\omega_i/2\pi \tag{19}$$

where, f_i is the ith natural frequency (cycles per unit time). Normalization of each eigenvector $\{\phi\}_i$ to the mass matrix is performed according to

$$\{\phi\}_i^T [M] \{\phi\}_i = 0 \tag{20}$$

In the normalization, $\{\phi\}_i$ is normalized such that its largest component is 1.0 (unity). The natural frequency of a structure is related to its geometry, mass, and boundary conditions. For the nanocones considered here, the mass was assumed to be that of each carbon atom, 2.0×10^{-26} kg, and the rotational degrees of freedom of the atom are neglected.

In the finite element modeling, the BEAM188 element in ANSYS was used to simulate the carbon bonds and the carbon atoms were simulated as the mass element of type MASS21. The authors have assumed that the cross-sections of the beam elements were uniform and circular, and the necessary input data of the BEAM188 element were the Young's modulus E, the Poisson's ratio m and the diameter of the circular cross-section d taken from Table 1.

Table 1. The input data prepared for the BEAM188 and MASS21 elements.

Division	Present work	Lee and Lee [28]
Beam Type	Euler-Bernoulli	Timoshenko
C–C bond length	0.142 nm	0.142
Poisson's ratio	0.3	0.3
Density	2.3×10^{-21} g/nm^3	2.3×10^{-27} kg/Å^3
Young's modulus	5448 nN/nm^2	5.448×10^{-8} N/Å^2
Shear modulus	-	8.701×10^{-9} N/Å^2
Mass of carbon atom	1.994×10^{-23} g	2×10^{-23} g

For the purpose of validating the Present model the results obtained are compared with Lee and Lee [28] as per Figure 4. Authors have considered nanocones with disclination angles are 120°, 180° and 240° and height of nanocones is 20 Å. A similar kind of trend is observed from the results of the presented model and Lee and Lee [28] with a difference in the values of frequencies quoted by Lee and Lee [28] and the current model. The reason can be attributed to the fact that the authors have used Euler Bernoulli beam theory without shear deformation whereas the one used by Lee and Lee [28] is Timoshenko beam element formulations which include shear deformation effects. The current methodology is based on Euler-Bernoulli beam element (i.e., see Table 1); this assumption affects the natural frequencies of SWCNC that are found to be lower than those of Euler-Bernoulli beam elements [37]. The results obtained are plotted, which show that the frequency variation between two model is not substantial and follows a similar trend in both the cases which suggests the validity of the present model and its further use.
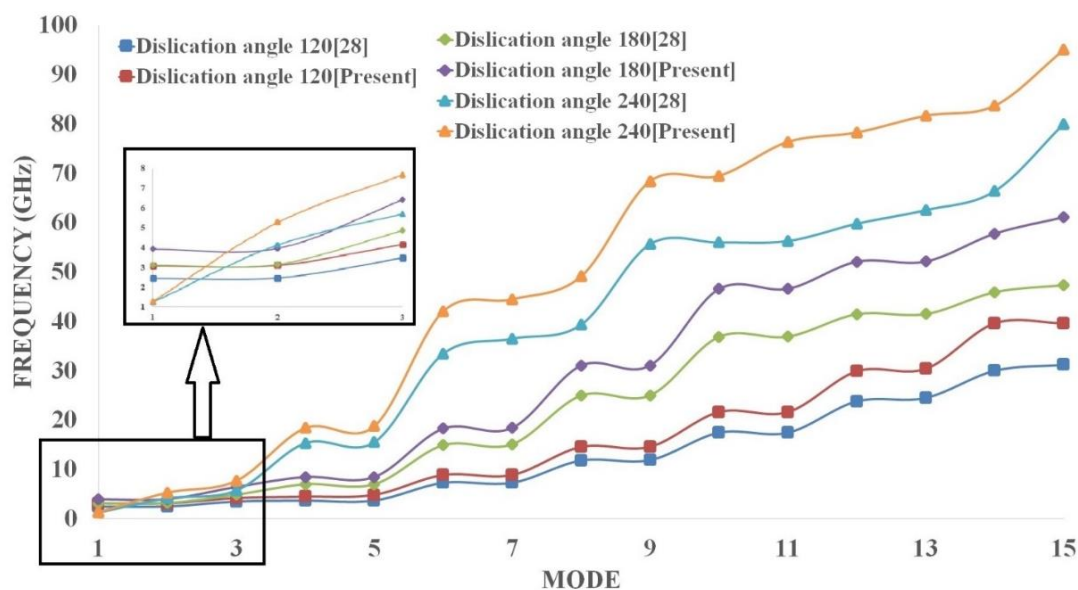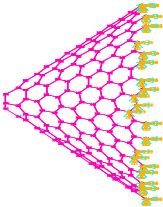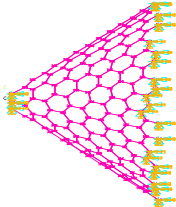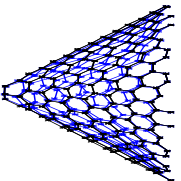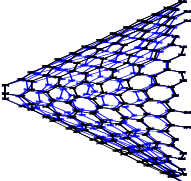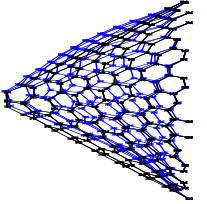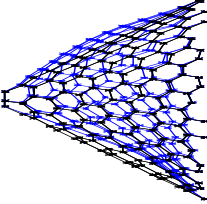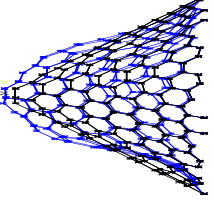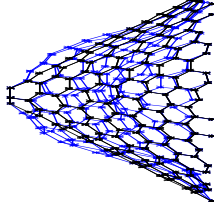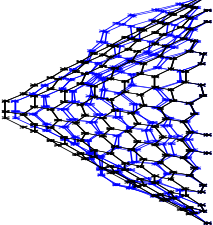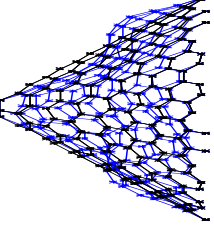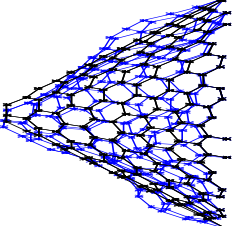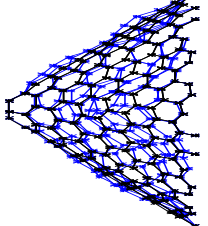
Figure 4. Comparison of first 15 mode of natural frequency for the SWCNCs with disclination angle 120 °, 180 ° and 240 ° between Lee and Lee [28] and Present Model.
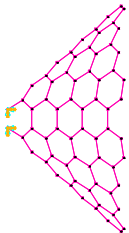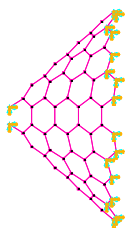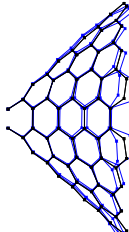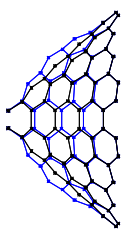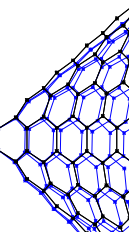
5. Results and Discussion
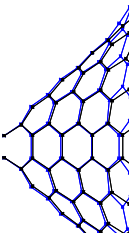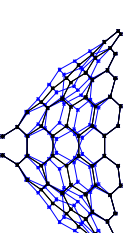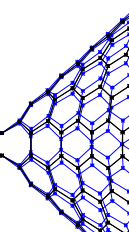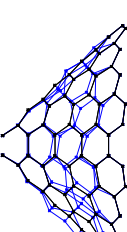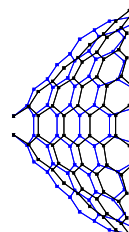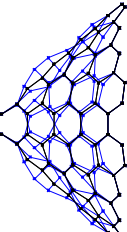
The nanocones with disclination angles of 60 °, 120 °, 180 ° and 240 ° and length of 10 Å with boundary condition of a cantilever and fixed beam were modelled as discussed above and shown in Tables 2–5.

The deformed shape of nanocones with 10 Å length and the four different disclination angles 60 °, 120 °, 180 ° and 240 ° are illustrated in Tables 2–5. The variations in natural frequency versus the mode of vibration for the cantilever and the fixed beam condition of nanocones with disclination angles 60 ° for all three lengths 10 Å, 15 Å and 20 Å is compared in Figures 5 and 6 separately. As presented in Figure 5, upto the mode 5 there is no significant change in the frequency for 15 Å and 20 Å length but for the smaller length 10 Å there is exponential change in frequency starting from mode 2. As presented in Figure 6, there is no significant change in frequency for all three lengths 10 Å, 15 Å and 20 Å upto the mode 5 than after there is major change in shorter length 10 Å. Subsequently, shorter length of SWCNC can be used for sensing application because of the wide range of frequency values. As the disclination is increased, there is significant change in frequency start from mode 4 for the shorter length of 120 ° disclination angle while for the 180 ° and 240 ° disclination angle change in frequency starting from mode 2 and mode 1 respectively. An increase in the frequency is observed when the disclination angle is increased, irrespective of the type of boundary condition. As shown in Figure 5, there is considerable difference observed between values of frequencies in modes 1–5 in fixed condition which is differ from cantilever condition as shown Figure 6. Similar kind of difference is observed in fixed and cantilever condition for disclination angle 120 °, 180 ° and 240 ° as shown in Figures 7–12.
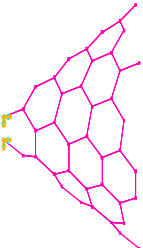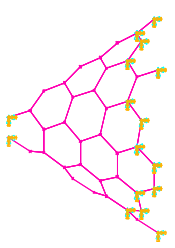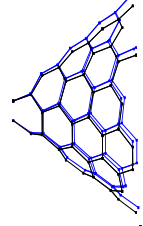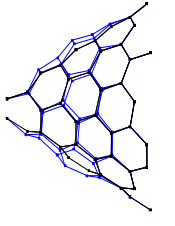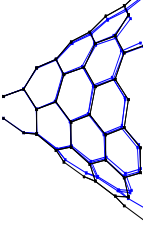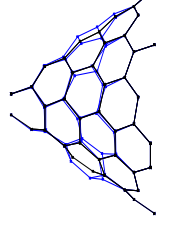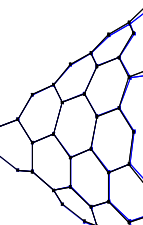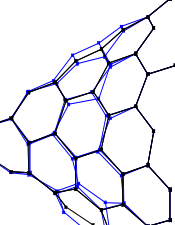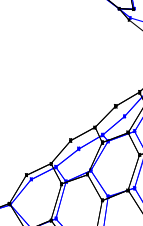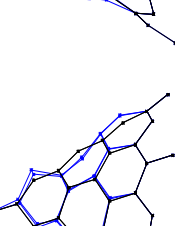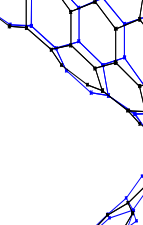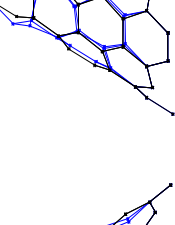
Table 2. Mode shapes of SWCNC (60 °angle and 10 Å Height).

	Cantilever	Bridge
320 Atoms, 455 Bonds		
Mode-1		
Mode-5		
Mode-10		
Mode-15		
Mode-20		
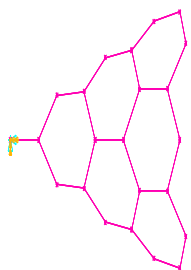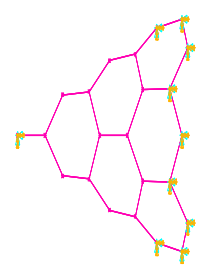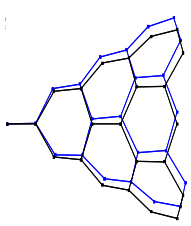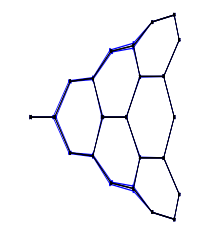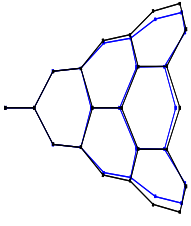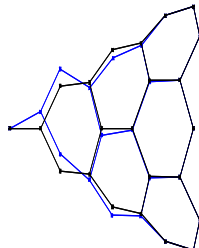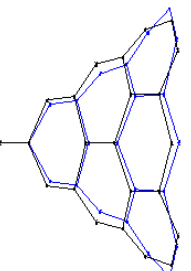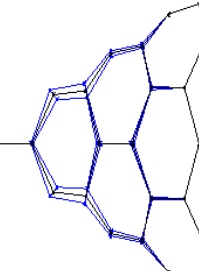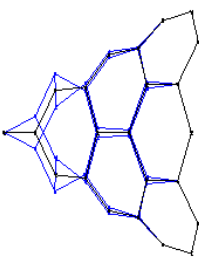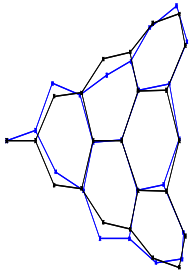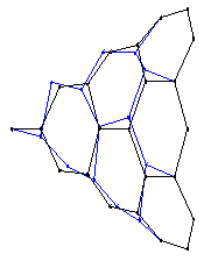
Table 3. Mode shapes of SWCNC (120 °angle and 10 Å Height).

	Cantilever	Bridge
136 Atoms, 192 Bonds		
Mode-1		
Mode-5		
Mode-10		
Mode-15		
Mode-20		

Table 4. Mode shapes of SWCNC (180 ° angle and 10 Å Height).

	Cantilever	Bridge
78 Atoms, 110 Bonds		
Mode-1		
Mode-5		
Mode-10		
Mode-15		
Mode-20		

Table 5. Mode shapes of SWCNC (240 ° angle and 10 Å Height).

	Cantilever	Bridge
46 Atoms, 63 Bonds		
Mode-1		
Mode-5		
Mode-10		
Mode-15		
Mode-20		
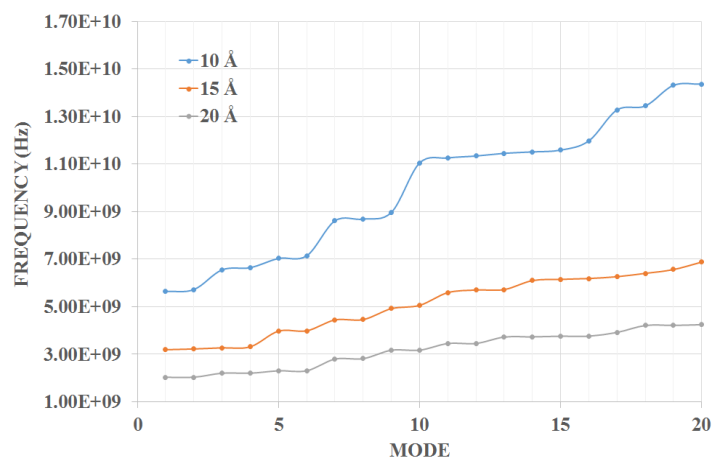
Figure 5. Variation in the natural frequency of SWCNCs with 60 ° and fixed beam for length of 10 Å, 15 Å and 20 Å.
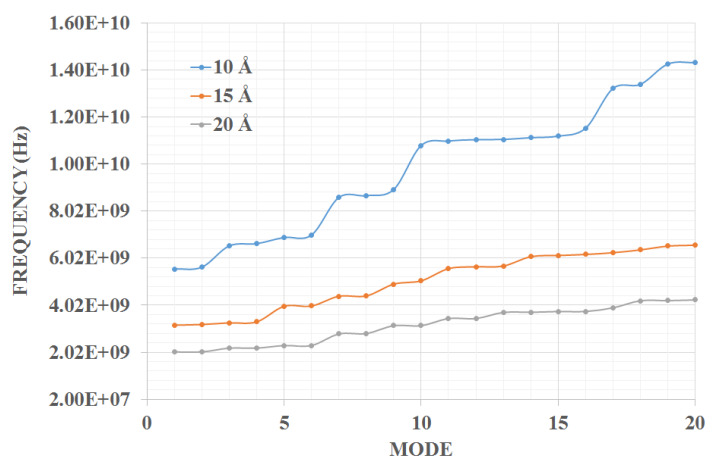
Figure 6. Variation in the natural frequency of SWCNCs with 60 ° and cantilever beam for length of 10 Å, 15 Å and 20 Å.
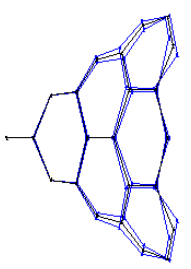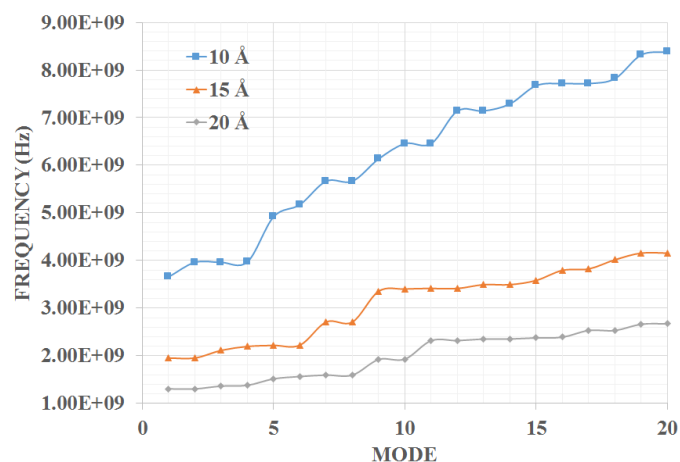

Figure 7. Variation in the natural frequency of SWCNCs with 120 ° and fixed beam for length of 10 Å, 15 Å and 20 Å.
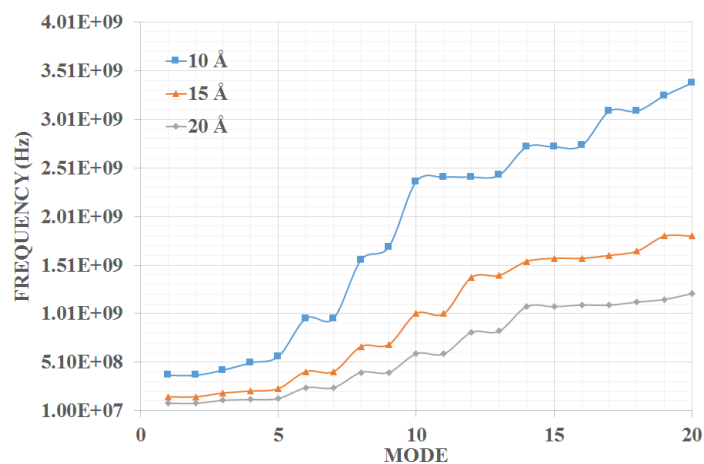
Figure 8. Variation in the natural frequency of SWCNCs with 120 ° and cantilever for length of 10 Å, 15 Å and 20 Å.
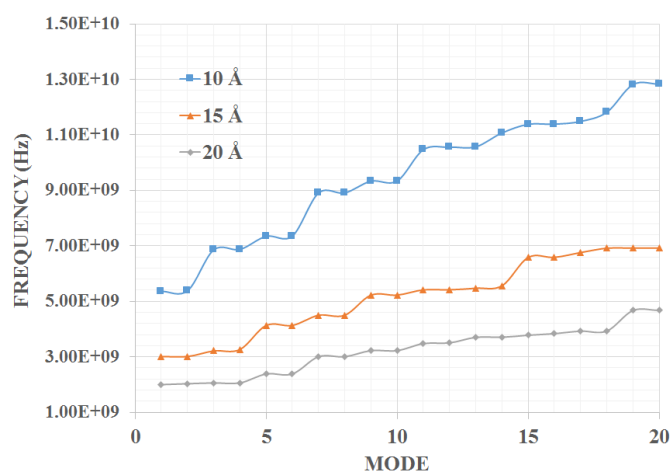
Figure 9. Variation in the natural frequency of SWCNCs with 180 ° and fixed beam for length of 10 Å, 15 Å and 20 Å.
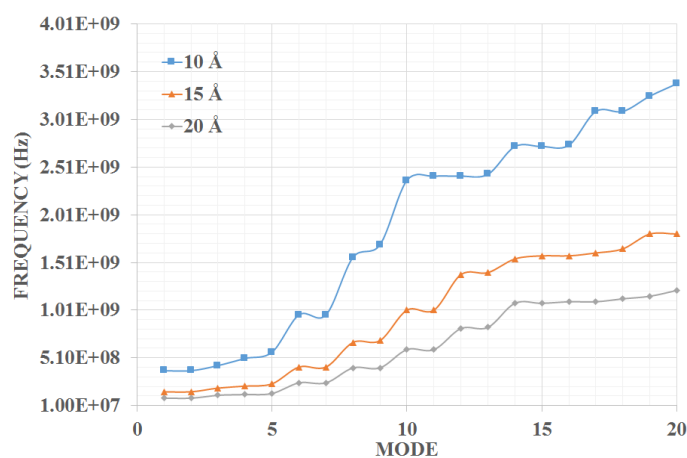
Figure 10. Variation in the natural frequency of SWCNCs with 180 ° and cantilever for length of 10 Å, 15 Å and 20 Å.
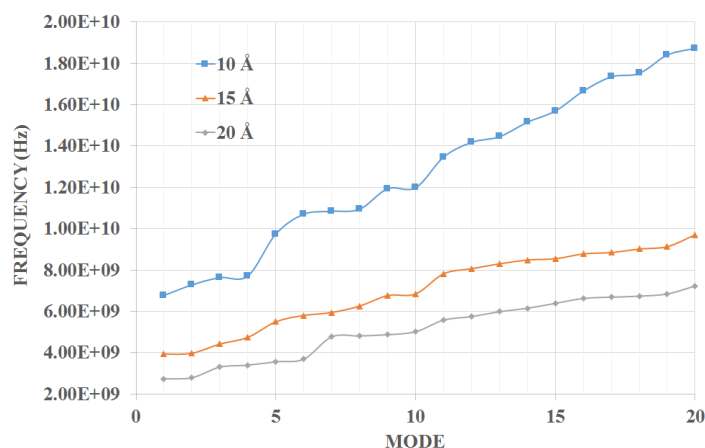
Figure 11. Variation in the natural frequency of SWCNCs with 240 ° and fixed beam for length of 10 Å, 15 Å and 20 Å.
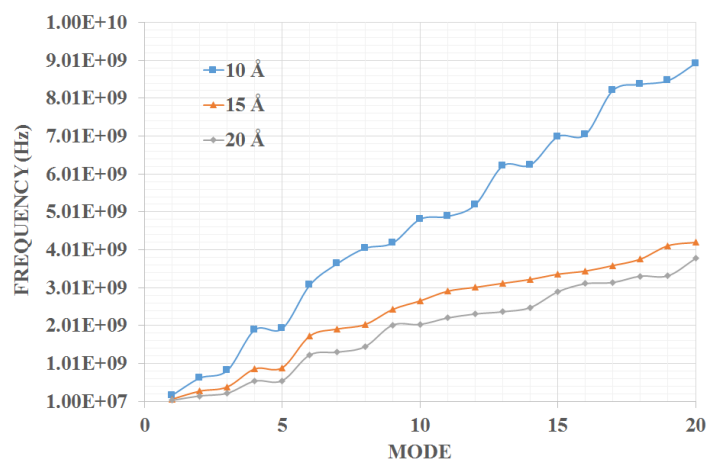
Figure 12. Variation in the natural frequency of SWCNCs with 240 ° and cantilever for length of 10 Å, 15 Å and 20 Å.

As can be seen, the frequency did not significantly differ for the first three modes of the cantilever or first two modes for the fixed, though, an unvarying pattern of variation was observed between the 10 Å and 15 Å length of SWCNC for higher vibrations.

As per the result for the fixed beam boundary conditions, it can be seen that frequencies are different for all mode shapes and they increase with increase in number of modes. From the results, it can be concluded that as the length increases the natural frequencies also decreases. SWCNC with 10 Å has much higher frequency compared with 15 Å and 20 Å in both boundary conditions.

The variations of the natural frequencies of the SWCNCs with apex angles of, 38.9 °, 60 ° and 86.6 °, 112.9 ° and for different boundary conditions are shown in Figures 5–12. It can be seen that natural frequency depend upon the apex angles as the apex angle decrease the frequency increases unrelated to the boundary condition.

The mode shape of deformation of nanocones shown in the table show that of SWCNC with the cantilever boundary condition experiences a similar bending as that of SWCNC with the fixed beam boundary condition.

6. Conclusion

The variation performance of SWCNCs with three different disclination angles 60°, 120°, 180° and 240° and for each angle, three different lengths 10 Å, 15 Å, and 20 Å were used in these studies. A combination of these variation in disclination and lengths were used for comparison for finding best sensing nanocone for sensing application. These models were used for modal analysis of two different boundary conditions fixed and cantilever beam to obtain different results for comparison of natural frequencies. The numerical analysis is reviewed as follows:

1) It was shown that increasing in disclination angle with constant length results in increasing in the frequency. Moreover, it was seen that the frequency value gap in mode 1 is decreasing when boundary condition change from fixed to cantilever for all three disclination angles.

2) It was shown that increasing the side length of a SWCNC with a constant apex angle result in decreasing the frequency. Moreover, it was seen that the SWCNCs with larger apex angles have smaller frequencies.

3) As can be seen, the frequencies did not significantly differ for the 15 Å and 20 Å lengths, and the first three modes of the cantilever or first two modes for the fixed boundary conditions. Furthermore, for the shorter length 10 Å frequencies are significantly changing from the first mode when increasing in the disclination angle for the both boundary conditions.

4) The mode of deformation demonstrated in Tables 2-5 shows that nanocone with disclination angle 240° have lesser number of atoms and bonds, is more physically stable than smaller disclination angle. Also, nanocones with more number of bonds and atom goes through more bending than large disclination.

5) The natural frequency of SWCNCs depends upon the apex angles, lengths and boundary condition for all modes of vibration.

Conflict of Interest

No potential conflict of interest is reported by the authors.

References

1. Iijima S (1991) Helical microtubules of graphitic carbon. *Nature* 354: 56.
2. Kroto HW, Heath JR, O'Brien SC, et al. (1985) C_{60}: Buckminsterfullerene. *Nature* 318: 162–163.
3. Kong XY, Ding Y, Yang R, et al. (2004) Single-crystal nanorings formed by epitaxial self-coiling of polar nanobelts. *Science* 303: 1348–1351.
4. Iijima S, Ichihashi T, Ando Y (1992) Pentagons, heptagons and negative curvature in graphite microtubule growth. *Nature* 356: 776.
5. Iijima S, Ichihashi T (1993) Single-shell carbon nanotubes of 1-nm diameter. *Nature* 363: 603–605.
6. Yu SS, Zheng WT (2010) Effect of N/B doping on the electronic and field emission properties for carbon nanotubes, carbon nanocones, and graphene nanoribbons. *Nanoscale* 2: 1069–1082.
7. Majidi R, Tabrizi KG (2010) Study of neon adsorption on carbon nanocones using molecular dynamics simulation. *Physica B* 405: 2144–2148.

8. Hu YG, Liew KM, He X, et al. (2012) Free transverse vibration of single-walled carbon nanocones. *Carbon* 50: 4418–4423.

9. Yan J, Liew KM, He L (2013) Ultra-sensitive analysis of a cantilevered single-walled carbon nanocone-based mass detector. *Nanotechnology* 24: 125703.

10. Krishnan A, Dujardin E, Treacy M, et al. (1997) Graphitic cones and the nucleation of curved carbon surfaces. *Nature* 388: 451.

11. Naess SN, Elgsaeter A, Helgesen G, et al. (2009) Carbon nanocones: wall structure and morphology. *Sci Technol Adv Mat* 10: 065002.

12. Iijima S, Brabec C, Maiti A, et al. (1996) Structural flexibility of carbon nanotubes. *J Chem Phys* 104: 2089–2092.

13. Yakobson B, Campbell M, Brabec C, et al. (1997) High strain rate fracture and C-chain unraveling in carbon nanotubes. *Comp Mater Sci* 8: 341–348.

14. S ánchez-Portal D, Artacho E, Soler JM, et al. (1999) Ab initio structural, elastic, and vibrational properties of carbon nanotubes. *Phys Rev B* 59: 12678.

15. Wang C, Tan V, Zhang Y (2006) Timoshenko beam model for vibration analysis of multi-walled carbon nanotubes. *J Sound Vib* 294: 1060–1072.

16. Hsu JC, Chang RP, Chang WJ (2008) Resonance frequency of chiral single-walled carbon nanotubes using Timoshenko beam theory. *Phys Lett A* 372: 2757–2759.

17. Zhang Y, Wang C, Tan V (2009) Assessment of Timoshenko beam models for vibrational behavior of single-walled carbon nanotubes using molecular dynamics. *Adv Appl Math Mech* 1: 89–106.

18. Ru C (2000) Effective bending stiffness of carbon nanotubes. *Phys Rev B* 62: 9973.

19. Yakobson BI, Brabec C, Bernholc J (1996) Nanomechanics of carbon tubes: instabilities beyond linear response. *Phys Rev Lett* 76: 2511.

20. Ru C (2000) Elastic buckling of single-walled carbon nanotube ropes under high pressure. *Phys Rev B* 62: 10405.

21. Odegard GM, Gates TS, Nicholson LM, et al. (2002) Equivalent-continuum modeling of nano-structured materials. *Compos Sci Technol* 62: 1869–1880.

22. Li C, Chou TW (2003) A structural mechanics approach for the analysis of carbon nanotubes. *Int J Solids Struct* 40: 2487–2499.

23. Rouhi S, Ansari R (2012) Atomistic finite element model for axial buckling and vibration analysis of single-layered graphene sheets. *Physica E* 44: 764–772.

24. Ansari R, Rouhi S (2010) Atomistic finite element model for axial buckling of single-walled carbon nanotubes. *Physica E* 43: 58–69.

25. Liew K, Lei Z, Yu J, et al. (2014) Postbuckling of carbon nanotube-reinforced functionally graded cylindrical panels under axial compression using a meshless approach. *Comput Method Appl M* 268: 1–17.

26. Zhang L, Lei Z, Liew K, et al. (2014) Static and dynamic of carbon nanotube reinforced functionally graded cylindrical panels. *Compos Struct* 111: 205–212.

27. Yan J, Liew KM, He L (2012) Predicting mechanical properties of single-walled carbon nanocones using a higher-order gradient continuum computational framework. *Compos Struct* 94: 3271–3277.

28. Lee J, Lee B (2012) Modal analysis of carbon nanotubes and nanocones using FEM. *Comp Mater Sci* 51: 30–42.

29. Fakhrabadi MMS, Khani N, Pedrammehr S (2012) Vibrational analysis of single-walled carbon nanocones using molecular mechanics approach. *Physica E* 44: 1162–1168.
30. Fakhrabadi MMS, Khani N, Omidvar R, et al. (2012) Investigation of elastic and buckling properties of carbon nanocones using molecular mechanics approach. *Comp Mater Sci* 61: 248–256.
31. Narjabadifam A, Vakili-Tahami F, Zehsaz M, et al. (2015) Three-dimensional modal analysis of carbon nanocones using molecular dynamics simulation. *J Vac Sci Technol B* 33: 051805.
32. Huang W, Xu J, Lu X (2016) Tapered carbon nanocone tips obtained by dynamic oxidation in air. *RSC Adv* 6: 25541–25548.
33. Patel AM, Joshi AY (2013) Vibration analysis of double wall carbon nanotube based resonators for zeptogram level mass recognition. *Comp Mater Sci* 79: 230–238.
34. Patel AM, Joshi AY (2014) Investigating the influence of surface deviations in double walled carbon nanotube based nanomechanical sensors. *Comp Mater Sci* 89: 157–164.
35. Jaszczak JA, Robinson GW, Dimovski S, et al. (2003) Naturally occurring graphite cones. *Carbon* 41: 2085–2092.
36. Lin CT, Lee CY, Chiu HT, et al. (2007) Graphene structure in carbon nanocones and nanodiscs. *Langmuir* 23: 12806–12810.
37. Baykasoglu C, Celebi AT, Icer E, et al. (2013) Vibration and elastic buckling analyses of single-walled carbon nanocones. 3rd South-East European Conference on Computational Mechanicsan ECCOMAS and IACM Special Interest Conference, Kos Island, Greece, 12–14.